Available online at www.sciencedirect.com
ScienceDirect
Scripta Materialia 61 (2009) 40–43
Scripta MATERIALIA
www.elsevier.com/locate/scriptamat

Electron irradiation-induced structural transformation in metallic glasses

E.G. Fu,[a] Jesse Carter,[b] Michael Martin,[b] Guoqiang Xie,[c] X. Zhang,[a] Y.Q. Wang,[d] Rick Littleton[e] and Lin Shao[b,*]

[a]*Department of Mechanical Engineering, Texas A&M University, College Station, TX 77843, USA*
[b]*Department of Nuclear Engineering, Texas A&M University, 129 Zachry, TAMU 3133, College Station, TX 77843, USA*
[c]*Institute for Materials Research, Tohoku University, Sendai 980-8577, Japan*
[d]*Los Alamos National Laboratory, Los Alamos, NM 87545, USA*
[e]*The Microscopy and Imaging Center, Texas A&M university, College Station, TX 77843, USA*

Received 6 February 2009; revised 1 March 2009; accepted 1 March 2009
Available online 6 March 2009

Microstructural evolution of $Zr_{55}Cu_{30}Al_{10}Ni_5$ and $Cu_{50}Zr_{45}Ti_5$ metallic glasses under 200 keV electron irradiation has been studied in situ by transmission electron microscopy. $Zr_{55}Cu_{30}Al_{10}Ni_5$, which has a wider supercooled liquid region, is found to be stable under electron irradiation and no crystallization is observed up to an irradiation fluence of 8.7×10^{26} electrons m^{-2}. In contrast, nanometer size crystalline $Cu_{10}Zr_7$ phases are formed in $Cu_{50}Zr_{45}Ti_5$ under electron irradiation. The partial crystallization is attributed to irradiation enhanced atomic mobility.

Keywords: Metallic glasses; Recrystallization

Extensive efforts have been made in the past few decades to develop high strength metallic glasses (MGs) [1–6]. Due to the lack of crystalline structures and grain boundaries, MGs exhibit high strength and high corrosion resistance. However, MGs have very poor ductility under stress [7]. Once shear bands are initialized, their uninhibited expansion easily leads to structural failure [7]. Introducing nanoscaled microstructures can increase materials toughness by arresting shear bands before causing structural failure [8–10]. It has been demonstrated that nanocrystal-dispersed MGs can effectively improve ductility [1]. Nanocrystal formation can be realized by annealing [11], deformation [12], bending [13], nanoindentation [14] and ion irradiation [15]. A few limited studies have demonstrated nanocrystal formation under electron irradiation [16–19]. However, details of the mechanisms of their nucleation and formation remain unclear. In this study, we investigated the microstructural evolution of $Zr_{55}Cu_{30}Al_{10}Ni_5$ and $Cu_{50}Zr_{45}Ti_5$ metallic glasses under electron irradiation. There are two reasons for selecting these materials: (i) both systems are well studied, with extensive literature on the crystallization kinetics, and they exhibit high mechanical strengths in the range 1700–2160 MPa [1] and (ii) we can examine the influence of crystallization temperature on electron irradiation stability given that $Zr_{55}Cu_{30}Al_{10}Ni_5$ has a higher crystallization temperature than $Cu_{50}Zr_{45}Ti_5$.

Ribbon samples of $Zr_{55}Cu_{30}Al_{10}Ni_5$ and $Cu_{50}Zr_{45}Ti_5$ metallic glasses, with a thickness of 20 μm and a width of 1.5 mm, were prepared by rapid solidification of metallic liquid on a rotating copper roller. Transmission electron microscopy (TEM) and high-resolution TEM were performed using a JEOL 2010 microscope equipped with a Gatan SC1000 ORIUS CCD camera, operated at 200 kV. The TEM specimens were prepared by electropolishing at 243 K using a twin jet thinning electropolisher with a solution of 25% nitric acid and 75% methanol. Differential scanning calorimetry (DSC) measurements were performed under a purified argon atmosphere in a TA Instruments DSC-Q1000 calorimeter with a finned air-cooling system.

Figure 1 compares DSC curves for as-spun $Zr_{55}Cu_{30}Al_{10}Ni_5$ and $Cu_{50}Zr_{45}Ti_5$ metallic glasses.

* Corresponding author. Tel.: +1 9798454107; fax: +1 9798456443; e-mail: lshao@mailaps.org

1359-6462/$ - see front matter © 2009 Acta Materialia Inc. Published by Elsevier Ltd. All rights reserved.
doi:10.1016/j.scriptamat.2009.03.001

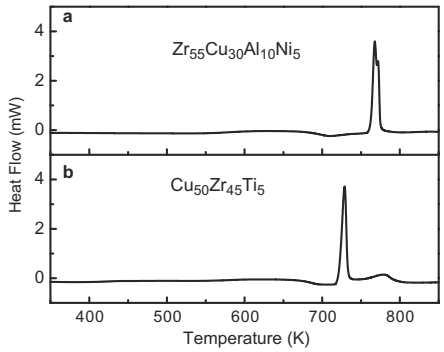

Figure 1. DSC traces of the as-spun metallic glasses before electron irradiation: (a) $Zr_{55}Cu_{30}Al_{10}Ni_5$; (b) $Cu_{50}Zr_{45}Ti_5$.

DSC was performed at a heating rate of 0.33 K s^{-1}. Glass transition temperatures were estimated to be 687 K for $Cu_{50}Zr_{45}Ti_5$ and 697 K for $Zr_{55}Cu_{30}Al_{10}Ni_5$. These temperatures correspond to the transition from glassy to supercooled liquid. At higher temperatures, the crystallization process starts involving nucleation and growth of crystalline phases. Figure 1 shows that the onset temperatures of the first-step crystallization are different for each MG. The crystallization temperature is around 722 K for $Cu_{50}Zr_{45}Ti_5$ and is 762 K for $Zr_{55}Cu_{30}Al_{10}Ni_5$. Thus, these two metallic glasses have different widths of the supercooled liquid region, which is a gauge to evaluate the thermal stability against crystallization [1]. A wider supercooled liquid region for the metallic glass $Zr_{55}Cu_{30}Al_{10}Ni_5$ indicates greater thermal stability against crystallization compared to metallic glass $Cu_{50}Zr_{45}Ti_5$.

Figures 2 and 3 compare TEM micrographs for metallic glass $Zr_{55}Cu_{30}Al_{10}Ni_5$ and $Cu_{50}Zr_{45}Ti_5$, respectively, subjected to 200 keV electron irradiation to different fluencies. Insets are the selected area diffraction (SAD) patterns for the corresponding TEM images. Figure 2a–c corresponds to $Zr_{55}Cu_{30}Al_{10}Ni_5$ after electron irradiation to $t = 0$, 15 and 30 min, respectively. The value t refers to the elapsed time after TEM characterization/electron irradiation started. Each image was taken within a few seconds. The specimen was continuously irradiated between each imaging. The electron beam was about 150 nm in diameter and the current density was around 11 A cm^{-2}. Therefore, the specimens shown in Figure 2a–c were irradiated to an electron fluence of 0, 4.4×10^{26} and 8.7×10^{26} electrons m^{-2}, respectively. In $Zr_{55}Cu_{30}Al_{10}Ni_5$ specimens irradiated at all three fluences, no crystalline phases were detected. SAD patterns in Figure 2a–c are maze-like with halo rings. This suggests that $Zr_{55}Cu_{30}Al_{10}Ni_5$ retains its glassy structure during electron irradiation.

Figure 3a–c shows microstructural changes of $Cu_{50}Zr_{45}Ti_5$ under electron irradiation of fluences of 0, 4.4×10^{26} and 8.7×10^{26} electrons m^{-2}, respectively. In Figure 3a, both the TEM image and the SAD pattern suggest the sample is in a glassy phase. After electron irradiation to a fluence of 4.4×10^{26} electrons m^{-2}, the SAD pattern in Figure 3b begins to show white diffraction dots, indicating the nucleation of nanocrystals. However, at this stage the size of the nanocrystals is very small, below the detection limit of TEM. After electron irradiation to a fluence of 8.7×10^{26} electrons m^{-2}, the

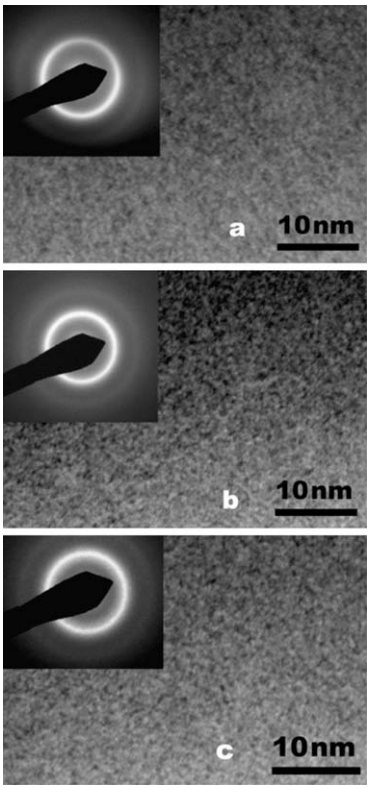

Figure 2. TEM micrographs of $Zr_{55}Cu_{30}Al_{10}Ni_5$ under 200 keV electron irradiation for (a) 0 min, (b) 15 min and (c) 30 min.

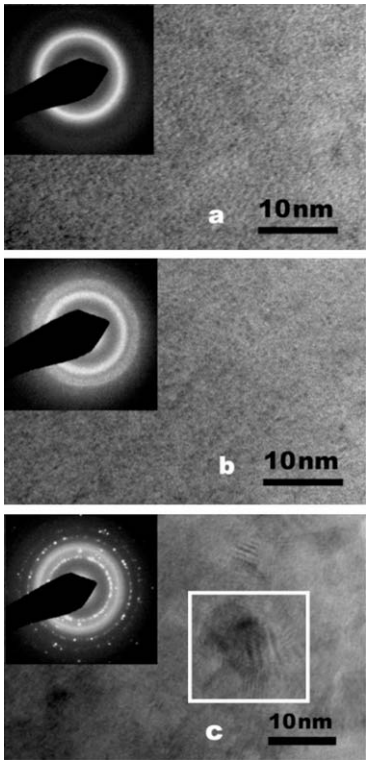

Figure 3. TEM micrographs of $Cu_{50}Zr_{45}Ti_5$ under 200 keV electron irradiation for (a) 0 min, (b) 15 min and (c) 30 min.

SAD pattern in Figure 3c clearly shows sharp diffraction spots and discontinuous diffraction rings. Nanocrystal formation is immediately apparent in the corresponding high-resolution TEM image. The typical size of the formed nanocrystals is around 10 nm.

Figure 4a shows the fast Fourier transform (FFT) pattern from the selected area (marked by the box in Fig. 3c). Indexing of the FFT pattern indicates the phase of nanocrystals to be predominantly $Cu_{10}Zr_7$; other minor phases are difficult to identify unambiguously from FFT. Figure 4b is an inverse FFT of a selected area in which a perfect nanocrystal is formed. In many other regions, defects such as dislocations are found to form in nanocrystals, as shown in a representative example in Figure 4c. Dislocations were counted using inverse FFT at different orientations (not shown here), which provided a dislocation density of $5 \times 10^{17}\ m^{-2}$.

The maximum recoil energy received by a target atom under a head-on collision can be calculate by [20]

$$E_{max} = \frac{4m_e ME}{(m_e + M)^2} \tag{1}$$

where E is the electron energy, m_e is the electron mass and M is the target atom's mass. The lightest atom will gain the highest knock-on energy. The maximum transferred energies are 9.1 eV for Ti and 16.2 eV for Al. Both energies are less than the displacement energies of their crystalline elemental materials ($E_d \approx 20\ eV$ for Ti and $E_d \approx 17\ eV$ for Al) [20]. However, Bellini et al. [21] has pointed out that the local displacement energy in glass is inversely correlated with the amount of free volume (FV), making it lower than that in the corresponding crystalline compound. Once atoms are displaced, vacancy-like defects are created, leading to the introduction of additional excessive FV and open space for atomic migration. Molecular dynamics simulation revealed that removing atoms from the structure result in a transient high-mobility region around the defects and a low mobility region, enabling the excessive FV to spread out over the whole sample over a longer time [22]. The diffusivity extracted from the simulation can be described by [22]

$$D = D_0 \exp(\Delta V_f / \Delta V_0) \tag{2}$$

where ΔV_0 is some activation volume. ΔV_f is the excess free volume introduced by removing atoms.

Based on the FV approaches originally introduced by Cohen and Turnbull [23] and later by Spaepen [24], it is expected that enhanced atomic mobility will lead to increased short-range order and subsequent nucleation. Therefore, irradiation-induced crystallization can occur at low temperature. However, due to the preferred displacements of light atoms by knock-on collisions, the irradiation enhanced displacement flux might be species dependent and the crystallization sequence could be different to thermal annealing.

It can be concluded that the electron-beam heating is negligible in this study. The temperature rises during electron irradiation can be estimated by [25]

$$\Delta T = \frac{I}{\pi k e}\left(\frac{dE}{dx}\right)\ln\frac{R}{r_0} \tag{3}$$

where k is the thermal conductivity ($k = 9$ W/mK for $Cu_{50}Zr_{45}Ti_5$ and 5 W/mK for $Zr_{55}Cu_{30}Al_{10}Ni_5$), $R(= 1.5$ mm) is the TEM specimen radius, $r_0(= 150$ nm) is the electron-beam radius, $I(= 12$ nA) is the beam current and dE/dx is the stopping power of electrons, which can be calculated by [26]

$$\frac{dE}{dx}(\text{keV/cm}) = -7.85 \times 10^4 \frac{Z\rho}{AE}\log\left(\frac{1.166 \times 200}{J}\right)$$
$$J(\text{keV}) = (0.76Z + 58.5Z^{-0.19}) \times 10^{-3} \tag{4}$$

where Z is the averaged atomic number, ρ is the density ($\rho = 7.23\ g\ cc^{-1}$ for $Cu_{50}Zr_{45}Ti_5$ and $6.83\ g\ cc^{-1}$ for $Zr_{55}Cu_{30}Al_{10}Ni_5$), A is the atomic weight ($g\ mol^{-1}$) and E is beam energy. The calculated stopping powers are 1.01 eV/nm for $Cu_{50}Zr_{45}Ti_5$ and 1.08 eV/nm for $Zr_{55}Cu_{30}Al_{10}Ni_5$. Substituting the values into Eq. (4) gives a temperature rise of 4.6 K for $Cu_{50}Zr_{45}Ti_5$ and 7.6 K for $Zr_{55}Cu_{30}Al_{10}Ni_5$. The electron-beam heating during irradiation is therefore negligible.

Formation of stable crystalline phases requires correlated atomic movements and rearrangements. Thus, crystallization is difficult if the nucleating phase has a complicated structure. Previous studies have shown that annealing of $Cu_{50}Zr_{45}Ti_5$ results in formation of the crystalline $Cu_{10}Zr_7$ phase. On the other hand, products of crystallized $Zr_{55}Cu_{30}Al_{10}Ni_5$ are very complicated. XRD analysis of annealed $Zr_{55}Cu_{30}Al_{10}Ni_5$ has identified tetragonal Zr_2Ni and $(Al_{1.7}Ni_{0.3})Zr$ intermetallic compounds, as well as several other unidentified phases [21]. Formation of multiple phases is believed to be the reason for the high stability of $Zr_{55}Cu_{30}Al_{10}Ni_5$ glass. Electron irradiation under the current conditions seems to be insufficient in overcoming the activation energy barrier to form multiple crystalline phases in amorphous $Zr_{55}Cu_{30}Al_{10}Ni_5$ glass.

After crystallization, continued irradiation will create defects in the newly formed nanocrystal, which results in

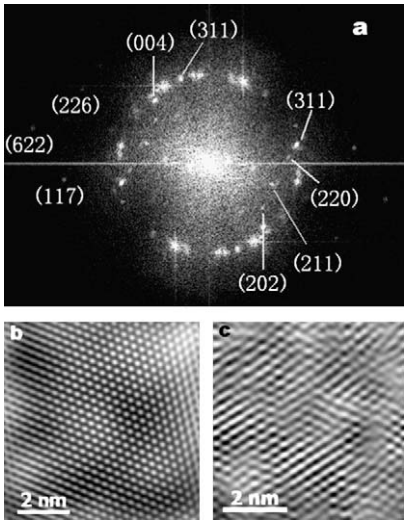

Figure 4. (a) FFT pattern of electron irradiated $Cu_{50}Zr_{45}Ti_5$ in the area marked in Figure 3c; (b) inverse FFT of a defect-free region; (c) inverse FFT of a region forming dislocations.

an increase in free energy (~5 eV for a Frenkel pair in face-centered cubic metal) [20]. Defects can also form in the as-grown nanocrystals without irradiation. If the free energy reaches a critical value, amorphization is possible [20]. The critical point defect concentration for this is estimated to be around 1% (atomic percentage) in metals [20], which is achievable under high fluence electron irradiation. However, the high free energy can be relieved through the formation of dislocations [27], which greatly lowers the maximum defect concentration in the system.

The stability of $Cu_{50}Zr_{45}Ti_5$ under electron irradiation has been previously studied by Xie et al. [19]. The crystalline phase was found to be monoclinic CuZr, rather than $Cu_{10}Zr_7$ phases identified in this study. In both studies, a number of weak unidentified phases are present, and coexistence of several phases is suggested. Formation of dominant phases might be sensitive to electron flux. In this study, the electron flux is $6.9 \times 10^{23}\ m^{-2}\ s^{-1}$, which is around one order of magnitude larger than the flux used in previous studies ($8 \times 10^{22}\ m^{-2}\ s^{-1}$).

Previous studies have suggested that the activation energy for nucleation is larger than the activation energy for crystal growth in amorphous alloys [28,29]. This has been used to explain the difference in shear-band-formation-induced nanocrystallization [29]. This study suggests that the activation energy for crystallization in $Zr_{55}Cu_{30}Al_{10}Ni_5$ is higher than that in $Cu_{50}Zr_{45}Ti_5$. However, once nucleation sites are introduced, these two glasses could have very different growth behaviors. In a separate study (to be published later), we have observed nanocrystal formation in both metallic glasses after high-energy Cu ion irradiation. Interestingly, once nucleation is initialized, crystal growth in $Zr_{55}Cu_{30}Al_{10}Ni_5$ is faster than that in $Cu_{50}Zr_{45}Ti_5$, which suggests that the activation energy for crystal growth in $Zr_{55}Cu_{30}Al_{10}Ni_5$ is comparable to, if not less than, that in $Cu_{50}Zr_{45}Ti_5$.

This study shows that a material's intrinsic property, i.e. width of the supercooled liquid region, affects its crystallization under electron irradiation. Thus it seems meaningful to carry out a comparison study in crystallization of amorphous alloys having different supercooled liquid widths under other conditions, including bending and deformation. A difference in their crystallization behavior might be observed.

From the viewpoint of application, electron irradiation can be used to modify bulk glass since high-energy electrons can penetrate through a large thickness. The technique has certain advantages over other techniques, such as shear-band-formation-induced nanocrystallization, since the latter phenomenon occurs after structural failure.

In summary, we have shown that $Zr_{55}Cu_{30}Al_{10}Ni_5$ has greater stability against crystallization than $Cu_{50}Zr_{45}Ti_5$ under electron irradiation. Irradiation with 200 keV electrons to a fluence of 8.7×10^{26} electrons m^{-2} results in the formation of $Cu_{10}Zr_7$ nanocrystals in $Cu_{50}Zr_{45}Ti_5$ metallic glass, but no crystallization is detected in $Zr_{55}Cu_{30}Al_{10}Ni_5$ metallic glass. Electron-beam heating is negligible. Furthermore, high-density dislocations are observed in crystalline $Cu_{10}Zr_7$ phases. This suggests that point defects in the system are highly mobile. Nucleation of dislocations is believed to be the mechanism to avoid the reamorphization of the formed crystalline phase.

This work was financially supported by the University Embryonic Technologies Program from Siemens Power Generation Emerging Technologies. L.S. acknowledges the support from the NRC Early Career Development Grant and the access to the user facilities at DOE-Center for Integrated Nanotechnologies (CINT). X.Z. acknowledges the support by DOE under grant number DE-FC07-05ID14657. Los Alamos National Laboratory, an affirmative action equal opportunity employer, is operated by Los Alamos National Security, LLC, for the National Nuclear Security Administration of the U.S. Department of Energy under contract DE-AC52-06NA25396.

[1] A. Inoue, Acta Mater. 48 (2000) 279.
[2] A. Peker, W.L. Johnson, Appl. Phys. Lett. 63 (1993) 2342.
[3] W.L. Johnson, MRS Bull. 24 (1999) 42.
[4] M.F. Ashby, A.L. Greer, Scr. Mater. 54 (2006) 321.
[5] A.I. Salimon, Mater. Sci. Eng. A 375 (2004) 385.
[6] A.L. Greer, Science 267 (1995) 1947.
[7] X. Rao, P.C. Si, J.N. Wang, Z. Xu, S. Xu, W.M. Wang, W.H. Wang, Mater. Lett. 50 (2001) 279.
[8] C.C. Hays, C.P. Kim, W.L. Johnson, Phys. Rev. Lett. 84 (2000) 2901.
[9] F. Szuecs, C.P. Kim, W.L. Johnson, Acta Mater. 49 (2001) 1507.
[10] D.C. Hofmann, J.-Y. Suh, A. Wiest, G. Duan, M.-L. Lind, M.D. Demetriou, W.L. Johnson, Nature 451 (2008) 1085.
[11] K. Lu, Mat. Sci. Eng. Rep. R16 (1996) 161.
[12] R. Schulz, M.L. Trudeau, D. Dussault, A. Van Neste, J. Phys. 51 (1990) C4259.
[13] H. Chen, Y. He, G.J. Shiflet, S.J. Poon, Nature 367 (1994) 6463.
[14] J.-J. Kim, Y. Choi, S. Suresh, A.S. Argon, Science 295 (2002) 654.
[15] R. Tarumi, K. Takashima, Y. Higo, Appl. Phys. Lett. 81 (2002) 4610.
[16] X.W. Du, M. Takeguchi, M. Tanaka, K. Furuya, Appl. Phys. Lett. 82 (2003) 1108.
[17] T. Nagase, Y. Umakoshi, Mater. Trans. 46 (2005) 616.
[18] A. Nino, T. Nagase, Y. Umakoshi, Mater. Trans. 46 (2005) 1814.
[19] G.Q. Xie, Q. Zhang, D.V. Louzguine-Luzgin, W. Zhang, A. Inoue, Mater. Trans. 47 (2006) 1930.
[20] M. Nastasi, J.W. Mayer, J.K. Hirvonen, Ion–Solid Interactions: Fundamentals and Applications, Cambridge University Press, New York, 1996.
[21] S. Bellini, A. Montone, M. Vittori-Antisari, Phys. Rev. B 50 (1994) 9803.
[22] V. Rosato, F. Cleri, J. Non-Crystalline Solids 144 (1992) 187.
[23] M.H. Cohen, D. Turnbull, J. Chem. Phys. 31 (1959) 1164.
[24] A. Van den Beukel, Acta Metall. Mater. 39 (1991) 2709.
[25] I. Jenčič, M.W. Bench, I.M. Robertson, M.A. Kirk, J. Appl. Phys. 78 (1995) 974.
[26] D.E. Newbury, R.L. Myklebust, Surf. Interface Anal. 37 (2005) 1045.
[27] Gary Was, Fundamentals of Radiation Materials Science, Springer, New York, 2007.
[28] K. Lu, J.T. Wang, Mater. Sci. Eng. A 133 (1991) 500.
[29] D.T.A. Matthews, V. Ocelík, P.M. Bronsveld, J.Th.M. De Hosson, Acta Mater. 56 (2008) 1762.